Experimental and Theoretical Characterization of Adsorbed Water on Self-Assembled Monolayers: Understanding the Interaction of Water with Atmospherically Relevant Surfaces†

Samar G. Moussa,‡ Theresa M. McIntire,‡ Milán Szőri,§ Martina Roeselová,§ Douglas J. Tobias,‡ Ronald L. Grimm,‡ John C. Hemminger,‡ and Barbara J. Finlayson-Pitts*,‡

Department of Chemistry, University of California, Irvine, California 92697-2025, and Center for Biomolecules and Complex Molecular Systems, Institute of Organic Chemistry and Biochemistry, Academy of Sciences of the Czech Republic, Flemingovo nám. 2, 16610 Prague 6, Czech Republic

Received: October 1, 2008; Revised Manuscript Received: December 2, 2008

A combination of experiments and molecular dynamic (MD) simulations has been applied to elucidate the nature of water on organic self-assembled monolayers (SAMs) before and after oxidation. SAMs mimic organics adsorbed on environmental urban surfaces. Water on clean or SAM-coated borosilicate glass surfaces was measured at equilibrium as a function of relative humidity (RH), using transmission Fourier transform infrared (FTIR) spectroscopy at 1 atm and 22 ± 1 °C. The SAMs included C18 and C8 alkanes, as well as the C8 terminal alkene. Oxidation of the terminal alkene SAM was carried out with either $KMnO_4$ solution or gaseous O_3. The FTIR data showed at least two distinct peaks due to water on these surfaces, one at ∼3200 cm^{-1}, which dominates at low RH (20%), and one at ∼3400 cm^{-1} at high RH (80%), which is similar to that in bulk liquid water. Temperature-programmed desorption (TPD) experiments showed that oxidation leads to more strongly adsorbed water. However, the amount of water in equilibrium with water vapor on the oxidized alkene was not significantly different from that on the unoxidized SAM, although there was a change in the relative intensities of the two contributing infrared peaks at 80% RH. MD simulations with hydrogen bond analysis suggest that molecules on the surface of small water clusters that dominate on SAM surfaces at low RH have fewer hydrogen bonds, while those in the interior of the clusters have three and four hydrogen bonds similar to bulk liquid water. Taken together, the experimental infrared data and MD simulations suggest a correlation between the relative intensities of the 3200 cm^{-1}/3400 cm^{-1} bands and the hydrogen-bonding patterns of the water on the surface and in the interior of clusters on the SAM surfaces. These studies suggest that water clusters will be present even on hydrophobic surfaces in the atmosphere and hence are available to participate in heterogeneous chemistry. In addition, oxidation of organic coatings on atmospheric particles or surfaces in the boundary layer may not lead to enhanced water uptake as is often assumed.

Introduction

Thin water films are found in the atmosphere on surfaces such as buildings, windows, vegetation, and airborne particles.[1−11] These surfaces are typically coated with a mixture of inorganic and organic compounds. The latter may be hydrophobic or hydrophilic, depending on the extent of oxidation. A molecular level understanding of the nature of water at such interfaces is critical since it may affect the kinetics and mechanisms of heterogeneous reactions on these surfaces.[3,12,13] In addition, the uptake of water on airborne particles is important for their growth and optical properties, and hence has impacts on radiative forcing and visibility.[14]

A prerequisite to understanding the chemical and physical impacts of these water films is characterization of the amount and nature of water on such surfaces. Water molecules at interfaces are believed to have unique structures different from those of bulk water.[1−4,15−28] The nature of interfacial water on different surfaces such as glass,[3,29,30] quartz,[3,4,26,27,31,32] salts,[1,33−35] metals[36−38] and metal oxides,[39−42] lipid membranes,[43] and hydrophobic and hydrophilic organic surfaces[18,19,21,22,24,25,28,44−57] has been the focus of many studies. Many of these studies identified at least two types of surface-adsorbed water molecules which have often been termed "ice-like" or "liquid-like". These depend on the amount of water and the nature of its interaction with the surface. For example, it has been proposed that there are distinct regions of water adsorbed on a silicon oxide surface: a more ordered "ice-like" structure layer at small water coverages, a less ordered liquid-like layer at larger water coverages, and a transition region between the two.[4,26,27] Although the term "ice-like" is frequently used to describe structured water at interfaces, this may be somewhat misleading. For instance, Verdaguer et al.[4] have shown that while the first one or two monolayers adsorbed on a silica surface are preferentially oriented by the substrate, the structure is not necessarily that of bulk ice. Similarly, Yang et al.[58−60] have proposed that water on hydroxylated silica surfaces forms a highly ordered 2-D structure consisting of quadrangular and octagonal hydrogen bonds, designated "ice tessellation".

Water on organic surfaces is particularly not well understood. This study presents a combined experimental and theoretical approach to understand adsorption of water on self-assembled monolayers (SAMs). SAMs are commonly used as proxies for organics adsorbed on surfaces and airborne dust particles.[14,52,61−66]

† Part of the "Max Wolfsberg Festschrift".

‡ University of California, Irvine.

§ Academy of Sciences of the Czech Republic.

* Author to whom correspondence should be addressed. E-mail: bjfinlay@uci.edu. Phone (949) 824-7670. Fax: (949) 824-2420.

10.1021/jp808710n CCC: $40.75
Published on Web 01/27/2009

Fourier transform infrared (FTIR) spectroscopy is used to characterize the position and intensity of the water infrared absorption bands in order to elucidate the nature of the hydrogen bonding and structure under equilibrium conditions. The data show that there is some water uptake at low relative humidities even on hydrophobic SAMs, with the water band red-shifted compared to bulk liquid water. At higher relative humidities, more water is adsorbed and the spectral signature approaches that of bulk liquid water. Oxidation of the monolayers did not substantially change these observations. Temperature-programmed desorption (TPD) studies give information about desorption energies and kinetics, providing insight into the nature of the water−surface interaction, and molecular dynamics (MD) simulations provide molecular level insights into the nature of water on these surfaces. The atmospheric implications of these findings are discussed.

We are particularly pleased to contribute this paper to the issue honoring Professor Max Wolfsberg whose seminal theoretical studies have contributed so much to the field of physical chemistry. Molecular dynamics simulations, interweaving of theory and experiments, and application to water in various environments have been topics of great interest to Professor Wolfsberg over the years, and we hope this contribution appropriately captures and celebrates a small portion of his contributions to this field.

Experimental Section

Surface Preparation. Thin borosilicate glass coverslips (VWR Micro cover, 25 mm in diameter, type I glass) were rinsed with purified water (Milli-Q Plus, 18.2 MΩ·cm), dried with nitrogen (Oxygen Service Co., 99.999%), and placed in an argon plasma discharge cleaner (Harrick Scientific Plasma Cleaner/Sterilizer PDC-32G, low power) for ∼10 min. These plasma-cleaned glass coverslips were rinsed with water, dried with nitrogen gas, and then placed in a 2 mM solution of alkyl trichlorosilane in hexadecane for 30 min to form the SAMs.[67] The SAM-coated coverslips were boiled 3 times in dichloromethane, wiped to remove residues, and then mounted in a holder described below for exposure to water. The alkane and alkene SAM precursors used were: C8 alkane (*n*-octyltrichlorosilane, Pfaltz and Bauer, Inc., 97%), C18 alkane (*n*-octadecyltrichlorosilane, Pfaltz and Bauer, Inc., 95%), and the C8 alkene (7-octenyltrichlorosilane, Sigma-Aldrich, mixture of isomers, 96%), designated as C8=. All the trichlorosilane precursors were used as received and the gases were ultrahigh purity (Oxygen Services Co., 99.999%).

The C8= SAMs were oxidized by using two different methods. In one method, the coated coverslips were mounted in a Teflon holder and placed in a collapsible thin film Teflon reaction chamber where they were exposed for 40 min to an O_3 concentration of $\sim(5-6) \times 10^{13}$ molecules cm^{-3}. Ozone was generated by the UV dissociation of O_2 (Oxygen Service Co., 99.993%) as described in detail elsewhere.[62] In the second method,[68−70] the C8= coated coverslips were mounted in a Teflon holder and placed overnight in an oxidizing solution consisting of a mixture of $KMnO_4$ (0.5 mM), $NaIO_4$ (19.5 mM), and K_2CO_3 (1.8 mM). The pH of K_2CO_3 was first adjusted to ∼7.5 with 1 M HCl. The coverslips were then removed and incubated in 0.3 M $NaHSO_3$ for 1 min, rinsed with water, and incubated for another 1 min in 0.1 M HCl to form carboxylic acid moieties. The coverslips were then rinsed with water and dried with N_2.

Contact Angles. The water contact angle was used to measure the wettability of the surfaces. A 1 μL droplet of water was deposited on the SAM-coated coverslips under ambient conditions and at a relative humidity of ∼60%. Pictures of the water droplet were taken with an Olympus C-5050 ZOOM digital camera.

Water Adsorption. Water adsorption on each surface was characterized as a function of relative humidity (RH), using transmission Fourier transform infrared (FTIR) spectroscopy (Mattson Galaxy 5020 FTIR, now Thermo Electron Corp., Madison, WI). Eleven glass coverslips (total of 22 surfaces) were mounted at 56° from normal incidence (Brewster's angle) in thin slots in a Teflon holder within a glass cell of 11 cm path length. A polarizer (Thorlabs Inc., WP25H-C) and a filter that eliminated radiation below 2000 cm^{-1} were placed between the infrared source and the cell. As discussed by Sumner et al.,[3] the optical filter was necessary to avoid a negative artifact peak at 3200 cm^{-1} caused by remodulation and phase shifting of the 1600 cm^{-1} water bend vibration. Desired water vapor concentrations, expressed throughout as relative humidities (RH), were achieved by mixing measured flows of dry and humid N_2 gas. Humid N_2 flows were obtained by bubbling dry nitrogen through water in two borosilicate fritted glass bubblers. The water bubblers were kept in a thermostated water bath. The temperatures of the room, cell, and water bath were kept constant at 22 ± 1 °C as measured by a thermocouple (OMEGA HH506).

All measurements were taken at a total pressure of 1 atm with a total gas flow of 200 mL min^{-1}. Background and sample transmission spectra were collected as 1024 single beam scans at 1.0 cm^{-1} resolution. Sample single beams at different RH were ratioed to the background single beams collected at 0% RH to generate sample absorption spectra. Water vapor absorption spectra at different RH were collected the same way but with the coverslips removed from the glass cell. The sample absorbance spectra were then corrected for water vapor at the desired relative humidity.

Temperature-Programmed Desorption (TPD) Experiments. Glass coverslips (Fisher Scientific, 12.5 mm in diameter, type I glass) were coated with trichlorosilanes as described above. The coated coverslips were afixed to a 1 cm diameter polished copper disk with a Torr Seal (Varian Inc.) and cured at 60 °C for 2 h under dry argon. The disk and coverslip were inserted into a UHV chamber with a temperature-controlled sample holder for desorption studies.[57] With a background pressure below 2×10^{-10} Torr, the sample was exposed to different doses of D_2O, which was used to minimize interference from background H_2O. Doses ranged from 0.1 to 6 L (1 Langmuir unit (1 L) = 10^{-6} Torr s^{-1}, 1 L exposure of water at 110 K approximates one monolayer (1 ML) of water, if the sticking coefficient is 1). Desorption experiments were performed at a constant heating rate of 3 K s^{-1}. The temperature was measured with a K-type thermocouple inserted into the copper disk. The D_2O desorption from the samples was monitored by using a quadrupole mass analyzer (UTI, model 100C) with a 70 eV electron impact ionization filament tuned to *m*/*z* 20.

Molecular Dynamic Simulations and Hydrogen Bond Analysis. MD simulations were used to model water uptake on SAMs composed of $-S(CH_2)_7CH_3$ and $-S(CH_2)_7COOH$ chains chemisorbed on a gold(111) surface. As in our previous work,[61] the use of alkylthiolates on gold in computer simulations rather than alkylsilanes on borosilicate glass substrate as in the experiment was motivated by methodological reasons. While potentials for accurately describing the interactions between alkanethiolates and the gold(111) surface are well established,[71] the relatively complex bonding between alkylsiloxanes and

silicon oxide surfaces introduces uncertainties in the development of atomistic models for alkylsiloxane SAMs.[72] Moreover, it has been shown that the structural differences between SAMs composed of long alkane chains on silica and on gold are minor.[73−75] For example, grazing incidence X-ray diffraction measurements have shown that alkyl chains of SAMs organize in two-dimensional hexagonal lattices with an area/chain of roughly 20 Å^2 and correlation lengths of tens of angstroms on both gold and silicon oxide surfaces.[76,77] In addition, contact angle measurements suggest very similar wetting behavior of hydrophobic SAMs formed from long-chain alkanes on gold and oxidized silicon substrates.[78,79] Since the main focus of this study is on the change of the organization of water molecules on SAM surface as the character of the surface is modified from hydrophobic (−CH_3 terminated SAM chains) to hydrophilic (−COOH terminated SAM chains), the structure and dynamics of water on these two types of SAM is likely to be affected primarily by the chemical nature of the end groups (−CH_3 vs −COOH) rather than by minor differences induced by different SAM substrates (silica vs gold). Thus, using a somewhat different SAM system as the computer model is not expected to affect significantly the resulting character of the SAM surfaces and their interactions with water.

Each monolayer consisted of 256 thiolate chains, arranged in a well-ordered, defect-free array of 16 × 16 chains with a surface area of ∼22 Å^2 per molecule. The simulation box dimensions were $x = 80.16$ Å, $y = 69.44$ Å, and $z = 90.00$ Å. The z dimension was perpendicular to the SAM/vapor interface with the (virtual) gold surface located at $z = 0$ Å. The vertical (z direction) thickness of the SAMs was approximately 13 Å. The CHARMM27 all-atom force field[80] was used to model the alkanethiolates, as in previous studies.[61,81,82] The interaction between the alkanethiolate chains and the gold substrate was modeled using the adsorption potential and surface corrugation potential, following the work of Mar and Klein.[71] Water was modeled using the SPC/E potential.[83]

Each of the SAMs described above was used in a series of MD simulations with varying numbers of water molecules meant to correspond to the conditions of the experiments reported in this paper. After 500 ps equilibration of the SAMs in the absence of water, five different amounts of water (33, 99, 232, 429, and 819 water molecules) were introduced into the simulation box, corresponding to a range from a submonolayer coverage to less than 2 water layers adsorbed on the SAM surface. MD simulations of each of the solvated systems were carried out for 3 ns. Atomic coordinates were saved every picosecond.

All of the simulations were performed with a constant number of molecules, volume, and temperature (NVT ensemble), using the NAMD 2.6 program.[84] The average system temperature, 300 K, was controlled by using the Langevin thermostat with the damping coefficient set to 1 ps^{-1}. Periodic boundary conditions were applied in all three dimensions. A reflecting wall (repulsive part of a Lennard-Jones potential) was placed in the xy plane at $z = 80$ Å to prevent the evaporated water molecules from crossing over the periodic boundary of the simulation box in the z direction. The cutoff for the van der Waals interactions and the real-space part of the electrostatic potential was set to 12 Å. The long-range electrostatic interactions were calculated by using the smooth Particle Mesh Ewald technique.[85] The equations of motion were integrated by using the Verlet algorithm with a time step of 1.0 fs. All bonds involving hydrogen atoms were constrained by using the SHAKE technique.[86]

TABLE 1: Assignment of the Infrared Bands for the Methylene Symmetric and Asymmetric Stretches and the and Full Width at Half Maximum (FWHM) for the Methylene Asymmetric Stretch

SAM	$\upsilon_{as}(CH_2)$, cm^{-1}	$\upsilon_{sy}(CH_2)$, cm^{-1}	fwhm cm^{-1}	refs
ordered film	2917	2848	14−16	91, 89
less-ordered film	2923	2856	23	61
C18	2915	2848	16	this study
C8	2920	2855	21	this study
C8=	2919	2850	21	this study

The hydrogen bond analysis was performed by averaging over the final 1000 ps of each trajectory. A hydrogen bond between a donor and acceptor water molecule was defined by using the following structural criteria: donor and acceptor oxygen atoms must be within 3.5 Å, and the angle between the vector connecting the donor and acceptor oxygens and the vector connecting the hydrogen and the acceptor oxygen must be less than 30°.[87] The analysis was performed with our own Tcl script in conjunction with the VMD program.[88]

Results and Discussion

a. Methyl Terminated Alkylsilane SAMs. Both the position and the full width at half-maximum (fwhm) of the absorbance peaks due to methylene symmetric, $\upsilon_{sy}(CH_2)$, and antisymmetric, $\upsilon_{as}(CH_2)$, stretches give insight into how well ordered the various monolayers are.[89] These frequencies are related to the population of the trans and gauche conformers in the alkyl chain, which translates into well-ordered and more disordered monolayers, respectively.[67,89−91] For closely packed chains in well-ordered monolayers,[89,91] the $\upsilon_{sy}(CH_2)$ is at 2848 cm^{-1} and $\upsilon_{as}(CH_2)$ is at 2917 cm^{-1}. However, for more disordered monolayers, these absorptions occur at ∼2856 and 2923 cm^{-1}, respectively. The bandwidth for well-ordered monolayers is ∼14−16 cm^{-1} and shifts to larger values as the alkyl chains become more disordered.[61] Table 1 shows the frequencies and bandwidths of the C8, C18, and C8= SAMs in the present study compared to several other studies. It is clear that the longer chain alkane C18 SAMs form a more ordered film compared to the shorter chain C8 alkane and C8= alkene SAMs, as expected due to stronger van der Waals interactions of the longer chain.

Figure 1 shows representative infrared spectra in the region of the OH stretching vibration of water on surfaces in equilibrium with low RH (20%), intermediate RH (40%), and high RH (80%). Also shown is a spectrum of bulk liquid water obtained by measuring the IR transmission through a water droplet sandwiched between two zinc selenide windows. The lines in the region above 3550 cm^{-1} are residuals due to subtraction anomalies of the temperature-sensitive narrow rotational lines of water vapor.[92]

Figure 1a shows water on plasma cleaned glass. There is only a weak, broad absorption in the 2900−3700 cm^{-1} region at relative humidities 20−40%, while at 80% RH, there is a band peaking at ∼3400 cm^{-1} that is very similar to that of bulk liquid water. Panels b and c of Figure 1 show the infrared spectra for the same substrate coated with C8 and C18 methyl terminated SAMs, respectively. There is a discernible peak around 3200 cm^{-1} that is evident at 20% and 40% RH in both cases. At 80% RH, there are contributions from both the 3200 and 3400 cm^{-1} peaks.

The observation at high RH of a peak at 3400 cm^{-1}, similar to that for bulk liquid water, is not surprising since water would be expected to "ball up" on a hydrophobic surface. This is

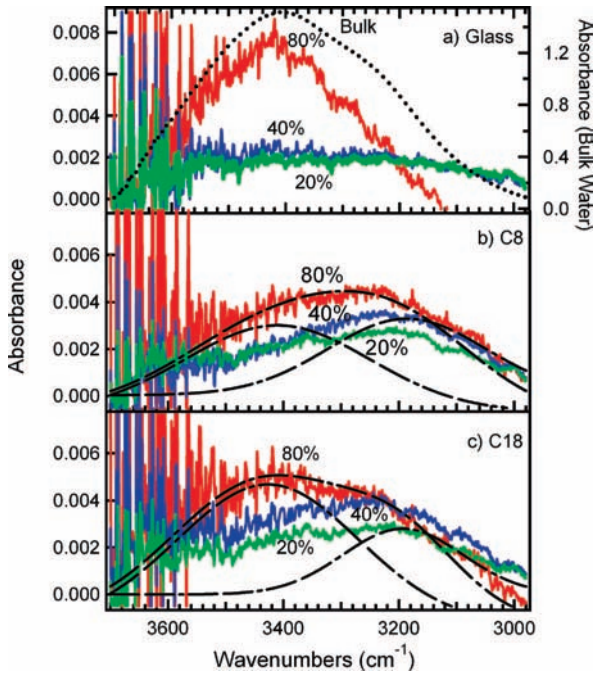

Figure 1. Infrared spectra of adsorbed water in equilibrium with water vapor at different percent RH on (a) plasma cleaned glass, (b) glass coated with a C8 SAM, and (c) glass coated with a C18 SAMs. The dotted line in panel a is the spectrum of bulk liquid water. The dashed lines in panels b and c represent the fitting of the 80% RH spectra into two peaks centered at 3200 and 3400 cm^{-1}, respectively. The different colors correspond to adsorbed water at different percent RH: green (20% RH), blue (40% RH), and red (80% RH).

reflected in the measured high contact angles: 107 ± 1° and 112 ± 2° for C8 and C18 SAMs, respectively. Water molecules in these droplets are strongly bound to each other and if the droplets are large enough, most of the water molecules in the interior are in an environment similar to that of bulk liquid water. The formation of large water clusters has also been predicted theoretically,[14,48,93,94] and is supported by MD simulations shown in Figure 2a for water on a hydrophobic, well-packed smooth C8 methyl terminated SAM. In 3 ns or less, starting from an initial configuration with water molecules spread over the surface, the water molecules formed a droplet on the surface, minimizing water−surface interactions and maximizing water−water interactions.

The relatively large contribution of the 3200 cm^{-1} band for the SAM-coated glass (Figure 1b,c) is interesting, given the hydrophobic nature of these surfaces and the predicted formation of droplets of water on them. However, sum-frequency generation (SFG) experiments with C18 SAMs on quartz also showed spectra with similar features in this region, in addition to a free OH stretch at ∼3680 cm^{-1}.[22,25,95] The 3200 cm^{-1} peak has been observed for water on bare silica surfaces and attributed to an "ice-like" or highly ordered structure due to hydrogen bonding to the surface −Si(OH) groups.[4,26,27,60,96] A similar ordering effect has been observed by other surfaces such as Pt(111) as well.[97]

This raises the possibility that the ordering of water on the hydrophobic surfaces leading to the appearance of the 3200 cm^{-1} peak is due to penetration of water molecules through to the substrate, especially on the more disordered C8 and C8= SAMs. Water has been observed to penetrate through SAMs,[25,63,89] particularly at defects and edges.[98] However, the differences in the shapes of the spectra of water on the substrate (Figure 1a) compared to the SAM coated substrates (Figure 1b,c) and the smaller amount of water taken up on the bare glass at 20−40% RH (0.8 ML compared to 1.5 ML on the coated glass at low RH) argue against this. In addition, one might expect this to be more important for the less ordered C8 alkane SAM, yet the water uptake at low RH is comparable in both SAM cases.

Another explanation is that water penetrates through the hydrocarbon chains and interacts with the new −Si(O)(O)− scaffolding introduced by the attachment of the SAM itself. This could give an ordered structure analogous to that induced by direct interaction with the −Si(OH) groups on the bare substrate. However, Ong et al.[99] showed that the interaction between water and buried oxygen in an alkoxy-terminated alkane thiol SAM ($HS(CH_2)_{16}O(CH_2)_nCH_3$) becomes weaker as n increases, and was undetectable for $n \geq 3$.

A third possibility is that small amounts of water on a hydrophobic surface are insufficient to form a larger droplet and instead form small, strained clusters whose hydrogen bonding differs from that of bulk liquid water. For example, some water clusters $(H_2O)_n$, where $n = 1-7$, have been reported to have structures that lead to a number of different infrared bands, including one at 3200 cm^{-1}, that reflect different patterns of hydrogen bonding.[100,101] Defects in the SAM could potentially trap small water clusters. One might then expect a stronger 3200 cm^{-1} band for the less ordered C8 alkane SAM. However, this is not observed (e.g., see the 80% RH spectra in panel b compared to that in panel c of Figure 1). Given that the infrared absorption bands for water in the condensed phase reflect coupled oscillations,[101−103] 2-D arrangements imposed by hydrogen bonding on the hydrophobic surface, perhaps similar to the ice tessellation structure,[58−60] seem possible as well.

To probe this further, a hydrogen bond analysis was performed on the MD trajectories. Figure 2b shows the probability that a water molecule forms a particular number of hydrogen bonds within a water droplet. The results from the simulations with a different number of water molecules are plotted in separate curves. In a droplet having only 33 water molecules, the highest probability is to form two hydrogen bonds (note that one monolayer of water in these simulations would correspond to 560 water molecules, assuming one water ML = 1×10^{15} molecule cm^{-2}).[104] As the number of water molecules in the MD simulation increases, the probability of forming three and to some extent four hydrogen bonds increases, with an almost equal probability of forming two or three hydrogen bonds for 99−429 water molecules. This is consistent with an average hydrogen bond coordination number for water molecules in bulk water of ∼3.5[17,105] dropping to ∼3.0[105] at the interface. For smaller droplets, a greater fraction of the water molecules are on the surface and make fewer hydrogen bonds, whereas hydrogen bonding in the interior of larger droplets should be similar to that of bulk water.

Figure 2c shows the probability of a water molecule forming a particular number of hydrogen bonds within the droplet as a function of increasing number of water molecules. At small numbers of water molecules, there is a probability of forming one or two hydrogen bonds [$P(1+2)$], which decreases as the probability of forming three to four hydrogen bonds [$P(3+4)$] becomes more favored for the larger clusters with more interior water molecules.

To relate the IR data to the MD simulations, curve fitting for the IR data was done with use of GRAMS/AI8 spectral data processing software (Thermo Electron Corp.). Spectra were fitted by using two overlapping peaks, one at 3400 cm^{-1} and another one at 3200 cm^{-1}, using Gaussian functions except for the samples oxidized with $KMnO_4$ where a Voigt function provided

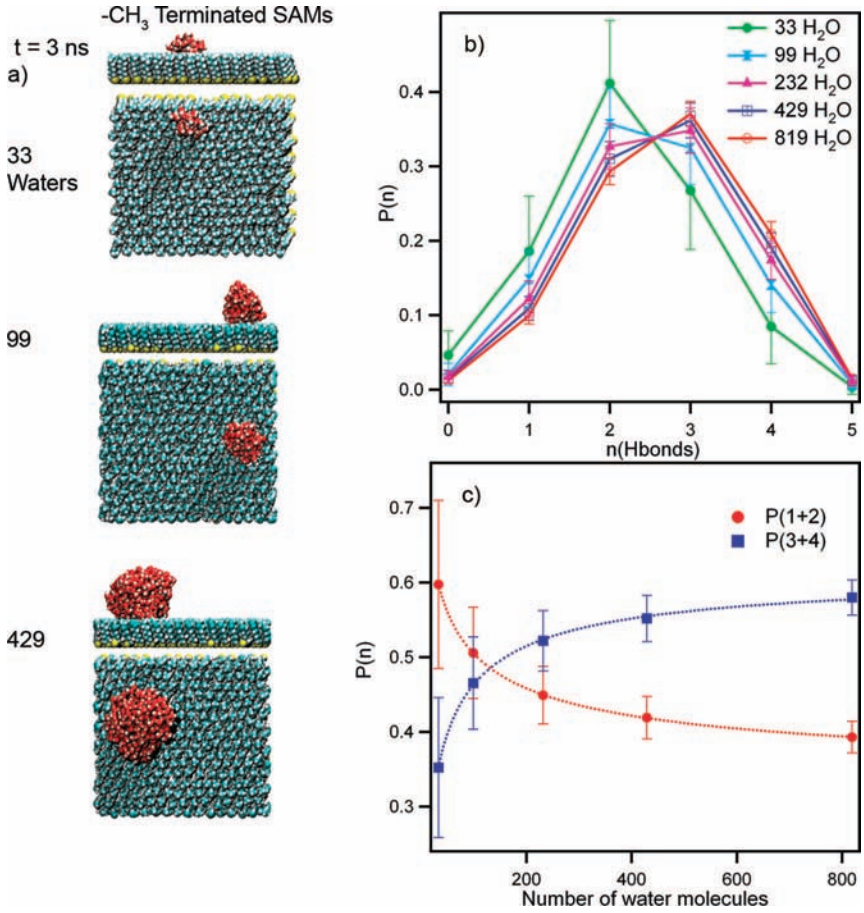

Figure 2. MD simulations of water on $-CH_3$ terminated C8 SAM: (a) side- and top-view snapshots for different numbers of water molecules at equilibrium; (b) probability distribution, $P(n)$, of a water molecule forming a particular number of hydrogen bonds, (c) $P(n)$ as a function of the number of water molecules.

a better fit. It should be noted that the choice of two peaks is somewhat arbitrary but including more than two does not significantly improve the fit and cannot be justified based on the experimental data. The equivalent number of liquid-like or structured water monolayers (Θ) was estimated from the IR spectra by using eq I,

$$\Theta = \frac{2.303A}{NS_{H_2O}\bar{\sigma}} \quad \text{(I)}$$

where N is the number of surfaces (total of 22) that are available to adsorb water, S_{H_2O} is the surface density of one water monolayer (1.0×10^{15} molecule cm^{-2}),[104] A is the integrated absorbance (base 10) for the peaks at 3400 or 3200 cm^{-1}, respectively, and $\bar{\sigma}$ is the integrated absorption cross section (base e) calculated by using the optical constants for water[106] or ice.[107] Obviously the description of the water responsible for the 3200 cm^{-1} band as ice at room temperature is not strictly representative; however, the use of ice optical constants for the 3200 cm^{-1} band provides a reasonable approach to estimate the number of structured water layers.

Figure 3 shows the fraction of the total water that is in a liquid-like or structured water configuration, respectively, as a function of RH, determined by curve fitting spectra such as those in Figure 1b,c. The total number of layers was obtained by adding the number of liquid-like water layers to the number of layers of structured water, each calculated from eq I with the appropriate absorption cross sections. As the RH increases, there is a shift toward an increasing fraction of liquid-like water. The overall trends do not change if the optical constants for liquid water are applied to the 3200 cm^{-1} band instead of those for ice. For example, Table 2 summarizes the equivalent number of monolayers of water and the corresponding fraction that is structured for C18 and C8 as a function of RH, using either the optical constants for ice for the 3200 cm^{-1} band (Figure 3) or those for liquid water. While the total number of equivalent monolayers of water is slightly larger for the assumption of liquid water optical constants, the fraction that is structured water

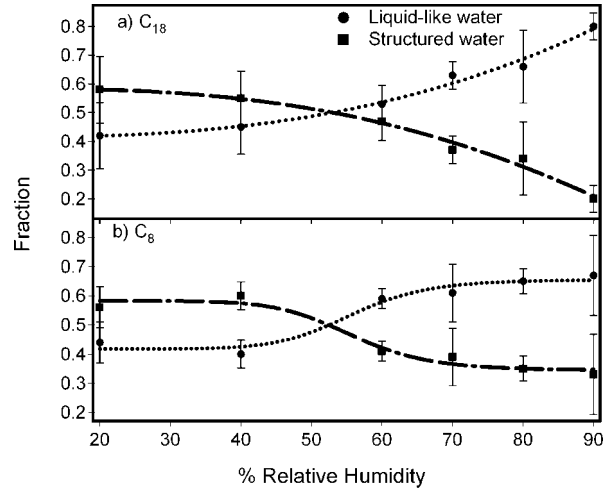

Figure 3. The fraction of the number of monolayers of liquid-like water and structured water on (a) C18 and (b) C8 as a function of RH, based on IR spectra such as those in Figure 1. The dotted and the dashed lines are fits to the actual data.

TABLE 2: Number of Equivalent Monolayers As a Function of RH and Corresponding Fractions of Structured Water on C18 and C8 SAMs, Using Either the Optical Constants for Ice or for Liquid Water

	with ice optical constants for the 3200 cm^{-1} band		with liquid water optical constants for the 3200 cm^{-1} band	
SAM/ %RH	equiv no. of ML ($\pm 2\sigma$)	fraction of structured water ($\pm 2\sigma$)	equiv no. of ML ($\pm 2\sigma$)	fraction of structured water ($\pm 2\sigma$)
C18				
20	0.94 ± 0.32	0.58 ± 0.22	1.32 ± 0.44	0.69 ± 0.20
40	1.14 ± 0.32	0.55 ± 0.18	1.57 ± 0.48	0.67 ± 0.18
60	1.35 ± 0.40	0.47 ± 0.14	1.78 ± 0.61	0.59 ± 0.12
70	1.71 ± 0.38	0.37 ± 0.10	2.14 ± 0.40	0.50 ± 0.10
80	1.80 ± 0.70	0.34 ± 0.26	2.08 ± 0.86	0.45 ± 0.28
90	2.34 ± 0.52	0.20 ± 0.10	2.66 ± 0.61	0.30 ± 0.12
C8				
20	0.88 ± 0.20	0.56 ± 0.14	1.22 ± 0.26	0.68 ± 0.12
40	1.05 ± 0.20	0.60 ± 0.10	1.4 ± 0.12	0.72 ± 0.08
60	1.39 ± 0.20	0.41 ± 0.06	1.78 ± 0.22	0.54 ± 0.06
70	1.57 ± 0.60	0.39 ± 0.20	1.99 ± 0.66	0.52 ± 0.20
80	1.64 ± 0.46	0.35 ± 0.08	2.03 ± 0.52	0.47 ± 0.10
90	1.83 ± 0.66	0.33 ± 0.28	2.23 ± 0.66	0.44 ± 0.30

is within experimental error for either assumption. MD simulations also predict that as the amount of water increases, the probabilities in the hydrogen bond distribution shift from lower to higher number of hydrogen bonds (Figure 2c).

Figure 4 shows representative snapshots from MD simulations of water on $-CH_3$ terminated C8 SAM, with each water oxygen atom color coded according to the number of hydrogen bonds in which the water molecule is involved. For each particular number of water molecules depicted in Figure 4, the snapshot was selected in such a way that the actual distribution of water molecules having a certain number of hydrogen bonds closely matches the average distribution (see Figure 2b). The color coding visually emphasizes that near the hydrophobic SAM surface as well as at the surface of the droplet exposed to the vapor phase, a majority of the water molecules form one to two hydrogen bonds, whereas in the interior of the droplet three to four hydrogen bonds are more common.

Direct comparison to previous work on the nature of water on hydrophobic surfaces is difficult as most of the earlier studies involve surfaces that were in direct contact with bulk liquid water. In contrast, the present studies involved submonolayer to 2 ML of water in equilibrium with water vapor. For example, Shen and co-workers[22,53,95] interpreted SFG data to mean that the 3200 cm^{-1} water peak on C18 covered silica was due to the hydrophobic SAM surface creating a rigid wall that forces water molecules to form a more ordered bonding network. Richmond and co-workers[56,108−112] have reported, based on vibrational sum frequency spectroscopic (VSFS) studies, that near a hydrophobic surface there is network of highly ordered, tetrahedrally coordinated water molecules that contributes to the 3200 cm^{-1} peak and less ordered asymmetrically bound water molecules that lead to the formation of the 3400 cm^{-1} peak. Consistent with this, MD simulations by Buch[113] attributed the 3400 cm^{-1} peak to surface water molecules with a coordination number of four, and the 3200 cm^{-1} peak to a mode that is delocalized over a few strongly coupled intermolecular hydrogen bonds of water molecules that are also predominantly four-coordinated. A theoretical study by Lee et al.[114] showed that near flat, hydrophobic surfaces, interfacial water has a structure similar to "Ice I" that minimizes water−surface

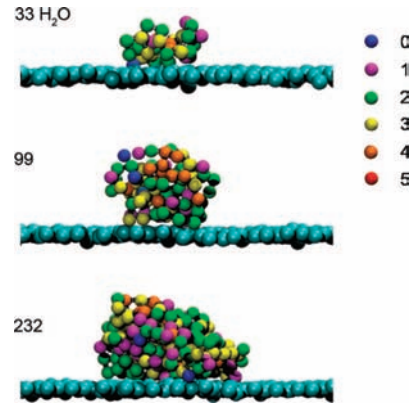

Figure 4. Representative snapshots from MD simulations of water on $-CH_3$ terminated C8 SAM, in which water oxygen atoms are color coded according to the number of hydrogen bonds each water molecule is participating in (see legend). For clarity, hydrogen atoms were removed and only water oxygen atoms and carbon atoms of the terminal $-CH_3$ groups of the SAM are shown.

interactions and maximizes water−water interactions. Their hydrogen bond analysis showed that the water nearest to the wall has about 75% as many hydrogen bonds as those in the bulk, qualitatively analogous to our analysis of hydrogen bonds for the small water clusters (Figures 2 and 4).

b. Oxidized SAM Coatings. One motivation for studying water on surfaces is to elucidate its role in heterogeneous chemistry in the atmosphere. Many of these environmental surfaces hold oxidized organics and hence water uptake on these is of interest. While it is commonly accepted that surfaces terminated with polar groups such as carboxylic acids will take up more water than hydrophobic surfaces, there are relatively few data in the literature to support this assumption. Most of the data that are available are for oxygen containing polar model compounds or relatively highly oxidized bulk films,[44,45,115] rather than on monolayer coatings.

To probe the amounts and nature of water on oxidized organic surfaces, C8= alkene SAMs were oxidized with ozone or $KMnO_4$ and exposed to increasing water vapor concentrations. Panels b and c of Figure 5 compare water uptake on such surfaces to that on the unoxidized C8= SAM (Figure 5a). On the basis of the absorbances, the total number of monolayers is 1.7 for the unoxidized SAM, which is within experimental error of the value of 1.6 for the ozonized film and 1.5 for the $KMnO_4$ oxidized SAM. It is striking there is no clear increase in the amount of water on the oxidized surface compared to the unoxidized SAM. This is in agreement with McIntire et al.,[62] who also reported no enhancement of water on ozone-reacted SAM coated quartz surfaces. The primary difference between the oxidized and unoxidized SAMs is that at 80% RH, the 3400 cm^{-1} peak attributed to liquid-like water on the surface contributes somewhat more to the spectrum on the oxidized surfaces (62% of the total surface coverage, compared to 56% for the unoxidized coating).

The products and mechanisms of ozonolysis of a terminal alkene SAM are complex.[14,61,64,65,116,117] In addition to the formation of carboxylic acids and aldehydes, cross polymerization to form large aggregates occurs.[62] These aggregates incorporate much of the organic material that was covering the substrate, leaving a surface that contains less organic than the unoxidized SAM.[62] The surface upon which water is being adsorbed in this case is therefore quite heterogeneous in nature.

To probe a more homogeneous but polar surface, the C8= SAM was also oxidized with $KMnO_4$ which is reported to generate a SAM that is fully terminated with −COOH groups.[68−70]

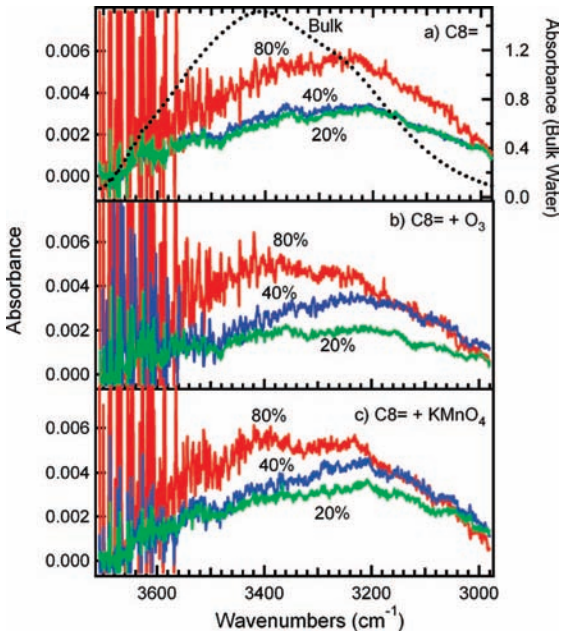

Figure 5. Infrared spectra of water on SAM-coated glass at different RH: (a) C8= unoxidized; (b) C8= oxidized with ozone; and (c) C8= oxidized with $KMnO_4$. The different colors correspond to adsorbed water at different percent RH: green (20% RH), blue (40% RH), and red (80% RH).

Figure 5c shows that the water on these surfaces is very similar to the surface oxidized by O_3 (Figure 5b). This result led us to consider whether instead of forming a −COOH terminated surface, other oxidation products are being generated. For example, Lemieux and von Rudloff [68,69] suggested that the permanganate−periodate oxidation of alkenes can proceed via many routes that involved different intermediates, which depending on the pH, can affect the oxidation process and final products. To verify that the $KMnO_4$ oxidized surface has carboxylic acid groups, a similar experiment was carried out on a silicon ATR crystal, which is transparent below 2000 cm^{-1}, unlike borosilicate glass. As seen in Figure 6, exposing the $KMnO_4$ oxidized SAM to NH_3 showed a decrease in the carbonyl group and the appearance of a carboxylate ion peak at 1555 cm^{-1} along with the formation of a broad ammonium feature in the 3300−3030 cm^{-1} region.[118] A similar conversion of −COOH to carboxylate on exposure to ammonia was reported for the ozonide C8= SAMs by Dubowski et al.[61]

While it is clear that the $KMnO_4$ oxidation generates −COOH groups, it is possible that the extent of conversion of the alkene groups is far from complete, and this could have an impact on the amount of water on the surface. However, comparing the net absorbance of the C=O peak before and after exposure to NH_3 showed that 84% of the surface is acid terminated upon oxidation with $KMnO_4$. To probe this further, temperature-programmed desorption experiments were also carried out.

c. TPD Experiments. TPD gives information about activation energies and overall kinetics of desorption, thus providing insight into the nature of the substrate−adsorbate interaction.[90] Figure 7 shows desorption of D_2O from a C8= alkene before and after oxidation with $KMnO_4$. TPD traces following 0.2 to 1.5 L D_2O exposures are shown with the 1.0 L trace shown in bold for both the unoxidized and the oxidized surface. The temperature range for water desorption from the unoxidized alkene surface was broad compared to studies of desorption from hydrophobic methyl-terminated surfaces[57,90,119,120] and the peak desorption temperature was higher than expected, ∼158 K for

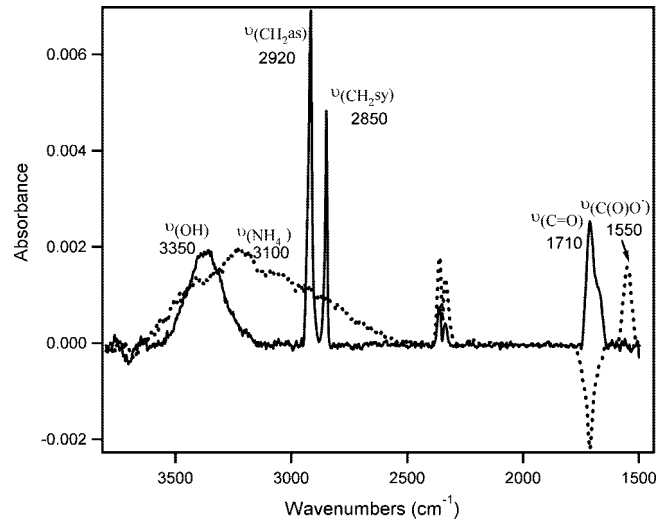

Figure 6. Infrared spectra of a C8= SAM oxidized with $KMnO_4$ on a silicon ATR crystal before (solid line) and after (dotted line) exposure to NH_3. The y-axis for the solid line is $\log(S_0/S_1)$, where S_1 and S_0 are the single beam spectra of C8= oxidized with $KMnO_4$ and plasma cleaned ATR crystal, respectively. The y-axis for the dotted line is $\log(S_1/S_2)$, where S_2 is the single beam spectrum of the C8= oxidized with $KMnO_4$ after exposure to NH_3.

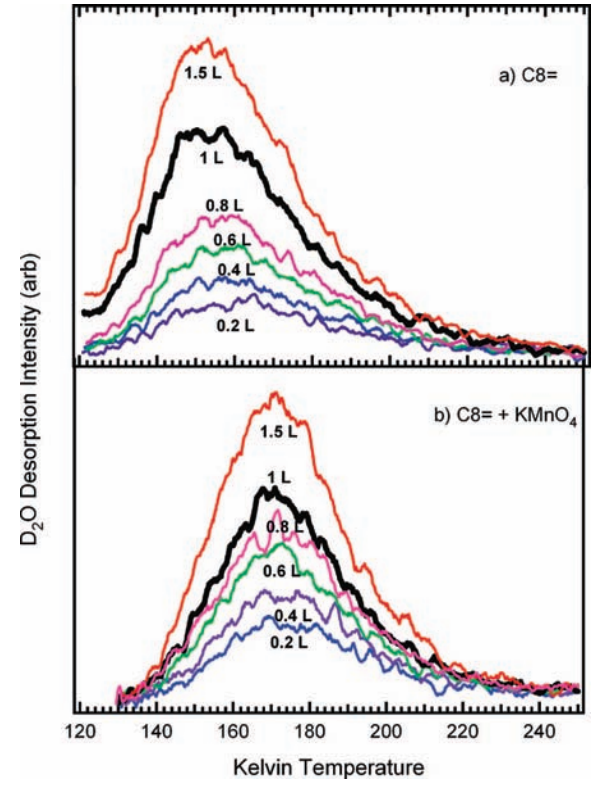

Figure 7. TPD spectra for desorption of various D_2O doses on (a) C8= unoxidized SAM and (b) C8= SAM oxidized with $KMnO_4$.

the 0.2 L water dose (a typical desorption peak temperature of water from hydrophobic thiol SAMs is around ∼140 K).[57,121] It is evident from the desorption traces in Figure 7a that the temperature at which the peak maxima occur shifts slightly to lower temperatures at higher coverages. Such behavior has also been reported for desorption from methyl terminated thiol SAM surfaces.[57]

The C8= SAM oxidized by either O_3 or $KMnO_4$ showed similar desorption profiles but for simplicity only desorption from the $KMnO_4$ oxidized surface is shown in Figure 7b.

Desorption of D_2O from the oxidized surface occurred at a higher temperature, ~176 K. The peaks were again broad at low coverages and narrowed slightly with increasing coverage. The peak temperatures remained approximately constant as a function of D_2O exposure.

The TPD results show that the interaction of water is stronger with the oxidized surfaces. Hydrogen bonding between water and hydrophilic SAMs has been discussed by a number of research groups.[57,90,119−126] The peak shape and coverage dependent shifts in the peak desorption temperatures are generally indicative of strong interlayer hydrogen-bonded interactions, especially at low coverages.[119,123] Comparison of these data to those of Grimm et al.[57] suggests that our surface is 75−90% oxidized, which is consistent with our estimate from the ammonia exposure experiment, and with the work of Wasserman et al.,[70] who reported that the $KMnO_4$ oxidation leads to an 80% −COOH terminated surface. In short, the lack of increased water uptake on the oxidized surfaces observed in FTIR studies cannot be due to small extents of oxidation of the SAMs.

As discussed elsewhere,[127,128] the temperature at which the peak desorption occurs can be used to estimate activation energies for desorption. However, there are some important caveats. All of the TPD desorption traces reported here were broad with a long tail that extended to high desorption temperatures. This suggests that the desorption rate may not be a simple first-order process and that the pre-exponential factor and activation energy (E_a) may be coverage dependent.[119] However, as a first approximation the desorption is assumed to be first order, and the pre-exponential factor is taken to be 1×10^{13} s^{-1}. This gives $E_a \approx 36 \pm 5$ kJ mol^{-1} for desorption of D_2O from the C18 SAM at a temperature of ~140 K with use of the 2 L data. This value is consistent with water adlayers forming three-dimensional water clusters, which have weak interactions with the surface.[57,119] For the unoxidized C8= SAM, an activation energy of 40 ± 6 kJ mol^{-1} at 158 K was obtained by using the 0.2 and 0.4 L data. On the other hand, E_a for the $KMnO_4$ and O_3 oxidized surfaces was $\sim 44 \pm 5$ kJ mol^{-1}, also with the 0.2 and 0.4 L data. This is significantly smaller than the 50 kJ mol^{-1} reported for a −COOH terminated thiol surface.[57] Given that the desorption process is very likely not a simple first-order kinetic process and the kinetic parameters are likely to be coverage dependent, care should be taken in the interpretation of these values for E_a. However, the values of E_a are good comparative measures of the relative strength of interaction of water with the various surfaces.

TPD was also carried out for the uncoated glass. The peak desorption temperature was even higher than that for the oxidized SAMs, ~205 K, which gives an activation energy for desorption of 50 ± 5 kJ mol^{-1}. This high desorption temperature and E_a for the substrate itself further suggests that in our experiments with the SAM coated glass, penetration of the water to the substrate is not a major factor for the SAM coated glass.

MD simulations again provide some insight into water on polar surfaces compared to the hydrophobic unreacted SAM. Figure 8 shows the results of simulations that are analogous to those shown in Figure 2, but for a −COOH terminated SAM. Note that in the absence of water, some hydrogen bonding occurs between the −COOH groups.[81,105,129] On the hydrophilic surface, water forms small clusters, but in contrast to the hydrophobic case, the clusters are distributed across the surface rather than coalescing into a larger droplet. As discussed by Winter et al.,[105] this is due to strong hydrogen bonding with the −COOH surface, where the probability of forming

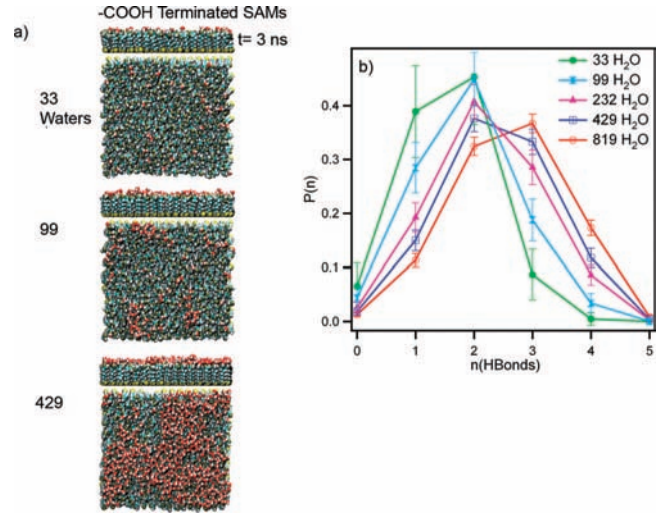

Figure 8. MD simulations of water on −COOH terminated C8 SAM: (a) side- and top-view snapshots for different numbers of water molecule at equilibrium and (b) probability distribution, $P(n)$, of a water molecule forming a particular number of hydrogen bonds. This represents the total probability, which includes hydrogen bonding to the substrate and to other water molecules.

water−COOH hydrogen bonds is larger than the probability of forming water−water hydrogen bonds.

Hydrogen bond analysis (Figure 8b) of water clusters on the hydrophilic SAM shows that at low coverage, the formation of one or two hydrogen bonds has the highest probability. These primarily represent hydrogen bonds between water and the carboxylic acid group.[105] As the number of water molecules increases, water−water interactions become more prominent, and the probability of forming three or four hydrogen bonds increases.

In summary, infrared spectra of water on hydrophobic and hydrophilic SAMs at room temperature display at least two different peaks, one that is similar to that of bulk liquid water and one that is red-shifted by ~200 cm^{-1}. Such a shift suggests the species responsible is more strongly hydrogen bonded than bulk liquid water, although the specific structure(s) that leads to this is not clear. In fact, a variety of structures with different intermolecular coupling may contribute.[15,101−103,113] According to the results of the MD simulations on the hydrophobic surface at low water coverages where the clusters formed are small, the formation of two hydrogen bonds is most probable. As the amount of water and size of the clusters increases, the formation of three hydrogen bonds becomes more important. Taken together, the experimental infrared data and MD simulations point to a correlation between the relative intensities of the 3200 cm^{-1}/3400 cm^{-1} bands and the hydrogen-bonding patterns in water clusters on the SAM surfaces. Thus, we hypothesize that water molecules involved in 1 or 2 hydrogen bonds on the surface of the clusters are associated with the 3200 cm^{-1} band and those with 3 or 4 hydrogen bonds in the interior of the cluster are associated with the 3400 cm^{-1} band. Calculations of infrared spectra from the MD trajectories will be required to confirm or refute this hypothesis.

On the −COOH terminated SAM, there is a significant probability of forming one hydrogen bond at low water coverage due to the interaction of water with −COOH groups, while water−water interactions with three hydrogen bonds become more important at higher water coverages. Although TPD studies show a slightly stronger interaction with the oxidized surfaces, the FTIR data show that the total amount of water at equilibrium is about the same as for the unoxidized SAM.

Atmospheric Implications

Silicates are a major component of environmental surfaces, e.g., surfaces of buildings and windows, as well as of airborne dust particles. In air, these surfaces become coated with a complex mixture of organic and inorganic species. The uptake of water on such surfaces is known to affect the heterogeneous reactions that take place on them.[3] In addition, water uptake also influences their radiative properties and their ability to form cloud condensation nuclei.[14,45,48,52]

Our data suggest that even purely hydrophobic surfaces adsorb some water that is then available for reaction. For example, Criegee intermediates formed in the ozonolysis reaction can be intercepted by water, changing the chemistry compared to that under dry conditions.[12,130] A common assumption is that as aerosols age in the atmosphere, i.e., hydrophobic organic compounds on the surface are oxidized by species such as OH, O_3, and NO_3, these surfaces will become more hydrophilic and take up more water.[14,52,131,132] However, the present studies showed that oxidation did not increase the amount of water on the surface, even for a surface that was more than 80% terminated by carboxylic acid groups. On the basis of their studies of oleic acid oxidation, Allen and co-workers[133] also argue against increased water uptake due to oxidation of surface organics. In that case, oxidation was shown to form smaller, volatile, or water-soluble species, leaving behind another hydrophobic coating.

In summary, water may play a more important role in heterogeneous chemistry on hydrophobic surfaces that were previously assumed not to have significant amounts of adsorbed water. On the other hand, it is clear that one cannot assume that water uptake will always be greater on oxidized surfaces compared to the parent organic. Whether the particular structure and bonding of water on these surfaces affect the heterogeneous chemistry on them remains to be explored. Clearly, further studies that provide molecular level insight into this interfacial chemistry and its implications for heterogeneous chemistry and particle growth in the atmosphere are needed.

Acknowledgment. The authors thank the National Science Foundation for support of this work through an Environmental Molecular Sciences Institute grant (0431312), S. Nizkorodov for the use of the CCD camera to measure contact angles, and Nicole M. Barrentine for assistance in the TPD experiments. We also thank K. J. Shea for helpful discussions regarding oxidation of alkene SAMs with the permanganate−periodate method. The work in Prague was supported by the Czech Science Foundation (Grant 203/06/1488) and the Ministry of Education of the Czech Republic (Grants 1P05ME798 and LC512), and was performed within the framework of the research project Z40550506.

References and Notes

(1) Ewing, G. E. *J. Phys. Chem. B* **2004**, *108*, 15953.
(2) Ewing, G. E. *Chem. Rev.* **2006**, *106*, 1511.
(3) Sumner, A. L.; Menke, E. J.; Dubowski, Y.; Newberg, J. T.; Penner, R. M.; Hemminger, J. C.; Wingen, L. M.; Brauers, T.; Finlayson-Pitts, B. J. *Phys. Chem. Chem. Phys.* **2004**, *6*, 604.
(4) Verdaguer, A.; Weis, C.; Oncins, G.; Ketteler, G.; Bluhm, H.; Salmeron, M. *Langmuir* **2007**, *23*, 9699.
(5) Diamond, M. L.; Gingrich, S. E.; Fertuck, K.; McCarry, B. E.; Stern, G. A.; Billeck, B.; Grift, B.; Brooker, D.; Yager, T. D. *Environ. Sci. Technol.* **2000**, *34*, 2900.
(6) Gingrich, S. E.; Diamond, M. L. *Environ. Sci. Technol.* **2001**, *35*, 4031.
(7) Lam, B.; Diamond, M. L.; Simpson, A. J.; Makar, P. A.; Truong, J.; Hernandez-Martinez, N. A. *Atmos. Environ.* **2005**, *39*, 6578.
(8) Law, N. L.; Diamond, M. L. *Chemosphere* **1998**, *36*, 2607.
(9) Gao, Y.; Anderson, J. R. *J. Geophys. Res., [Atmos.]* **2001**, *106*, 18037.
(10) Seinfeld, J. H.; Carmichael, G. R.; Arimoto, R.; Conant, W. C.; Brechtel, F. J.; Bates, T. S.; Cahill, T. A.; Clarke, A. D.; Doherty, S. J.; Flatau, P. J.; Huebert, B. J.; Kim, J.; Markowicz, K. M.; Quinn, P. K.; Russell, L. M.; Russell, P. B.; Shimizu, A.; Shinozuka, Y.; Song, C. H.; Tang, Y. H.; Uno, I.; Vogelmann, A. M.; Weber, R. J.; Woo, J. H.; Zhang, X. Y. *Bull. Am. Meteorol. Soc.* **2004**, *85*, 367.
(11) Falkovich, A. H.; Schkolnik, G.; Ganor, E.; Rudich, Y *J. Geophys. Res.* **2004**, *109*, D02208; doi:10.1029/2003JD003919.
(12) Finlayson-Pitts, B. J.; Pitts, J. N., Jr. *Chemistry of the Upper and Lower Atmosphere: Theory, Experiments and Applications*; Academic Press: San Diego, CA, 2000.
(13) Finlayson-Pitts, B. J.; Wingen, L. M.; Sumner, A. L.; Syomin, D.; Ramazan, K. A. *Phys. Chem. Chem. Phys.* **2003**, *5*, 223.
(14) Rudich, Y. *Chem. Rev.* **2003**, *103*, 5097.
(15) Tian, C.; Ji, N.; Waychunas, G. A.; Shen, Y. R. *J. Am. Chem. Soc.* **2008**, *130*, 13033.
(16) Lutzenkirchen, J.; Preocanin, T.; Kallay, N. *Phys. Chem. Chem. Phys.* **2008**, *10*, 4946.
(17) Bagchi, B. *Chem. Rev.* **2005**, *105*, 3197.
(18) Gragson, D. E.; McCarty, B. M.; Richmond, G. L. *J. Phys. Chem.* **1996**, *100*, 14272.
(19) Gragson, D. E.; McCarty, B. M.; Richmond, G. L. *J. Am. Chem. Soc.* **1997**, *119*, 6144.
(20) Henderson, M. A. *Surf. Sci. Rep.* **2002**, *46*, 5.
(21) Richmond, G. L. *Chem. Rev.* **2002**, *102*, 2693.
(22) Shen, Y. R.; Ostroverkhov, V. *Chem. Rev.* **2006**, *106*, 1140.
(23) Thiel, P. A.; Madey, T. E. *Surf. Sci. Rep.* **1987**, *7*, 211.
(24) Verdaguer, A.; Sacha, G. M.; Bluhm, H.; Salmeron, M. *Chem. Rev.* **2006**, *106*, 1478.
(25) Ye, S.; Nihonyanagi, S.; Uosaki, K. *Phys. Chem. Chem. Phys.* **2001**, *3*, 3463.
(26) Asay, D. B.; Kim, S. H. *J. Phys. Chem. B* **2005**, *109*, 16760.
(27) Hasegawa, T.; Nishijo, J.; Imae, T.; Huo, Q.; Leblanc, R. M. *J. Phys. Chem. B* **2001**, *105*, 12056.
(28) Ma, G.; Chen, X. K.; Allen, H. C. *J. Am. Chem. Soc.* **2007**, *129*, 14053.
(29) Garbatski, U.; Folman, M. *J. Chem. Phys.* **1954**, *22*, 2086.
(30) Michel, D.; Kazansky, V. B.; Andreev, V. M. *Surf. Sci.* **1978**, *72*, 342.
(31) Dubowski, Y.; Sumner, A. L.; Menke, E. J.; Gaspar, D. J.; Newberg, J. T.; Hoffman, R. C.; Penner, R. M.; Hemminger, J. C.; Finlayson-Pitts, B. J. *Phys. Chem. Chem. Phys.* **2004**, *6*, 3879.
(32) Li, I.; Bandara, J.; Shultz, M. J. *Langmuir* **2004**, *20*, 10474.
(33) Foster, M. C.; Ewing, G. E. *J. Chem. Phys.* **2000**, *112*, 6817.
(34) Peters, S. J.; Ewing, G. E. *J. Phys. Chem. B* **1997**, *101*, 10880.
(35) Peters, S. J.; Ewing, G. E. *Langmuir* **1997**, *13*, 6345.
(36) Jo, S. K.; Kiss, J.; Polanco, J. A.; White, J. M. *Surf. Sci.* **1991**, *253*, 233.
(37) Ogasawara, H.; Yoshinobu, J.; Kawai, M. *Chem. Phys. Lett.* **1994**, *231*, 188.
(38) Yamamoto, S.; Beniya, A.; Mukai, K.; Yamashita, Y.; Yoshinobu, J. *J. Phys. Chem. B* **2005**, *109*, 5816.
(39) Al-Abadleh, H. A.; Grassian, V. H. *Langmuir* **2003**, *19*, 341.
(40) Daschbach, J. L.; Dohnalek, Z.; Liu, S. R.; Smith, R. S.; Kay, B. D. *J. Phys. Chem. B* **2005**, *109*, 10362.
(41) Foster, M.; Furse, M.; Passno, D. *Surf. Sci.* **2002**, *502*, 102.
(42) Foster, M.; Passno, D.; Rudberg, J. *J. Vac. Sci. Technol. A* **2004**, *22*, 1640.
(43) Binder, H. *Eur. Biophys. J.* **2007**, *36*, 265.
(44) Asad, A.; Mmereki, B. T.; Donaldson, D. J. *Atmos. Chem. Phys.* **2004**, *4*, 2083.
(45) Demou, E.; Visram, H.; Donaldson, D. J.; Makar, P. A. *Atmos. Environ.* **2003**, *37*, 3529.
(46) Donaldson, D. J.; Vaida, V. *Chem. Rev.* **2006**, *106*, 1445.
(47) Mamatkulov, S. I.; Khabibullaev, P. K.; Netz, R. R. *Langmuir* **2004**, *20*, 4756.
(48) Rudich, Y.; Benjamin, I.; Naaman, R.; Thomas, E.; Trakhtenberg, S.; Ussyshkin, R. *J. Phys. Chem. A* **2000**, *104*, 5238.
(49) Schwendel, D.; Hayashi, T.; Dahint, R.; Pertsin, A.; Grunze, M.; Steitz, R.; Schreiber, F. *Langmuir* **2003**, *19*, 2284.
(50) Sharp, K. A.; Madan, B.; Manas, E.; Vanderkooi, J. M. *J. Chem. Phys.* **2001**, *114*, 1791.
(51) Takei, T.; Yamazaki, A.; Watanabe, T.; Chikazawa, M. *J. Colloid Interface Sci.* **1997**, *188*, 409.
(52) Thomas, E.; Rudich, Y.; Trakhtenberg, S.; Ussyshkin, R. *J. Geophys. Res.* **1999**, *104*, 16053.
(53) Miranda, P. B.; Shen, Y. R. *J. Phys. Chem. B* **1999**, *103*, 3292.
(54) Michot, L. J.; Villieras, F.; Francois, M.; Bihannie, I.; Pelletier, M.; Cases, J. M. *C. R. Geosci.* **2002**, *334*, 611.
(55) Konek, C. T.; Musorrafiti, M. J.; Al-Abadleh, H. A.; Bertin, P. A.; Nguyen, S. T.; Geiger, F. M. *J. Am. Chem. Soc.* **2004**, *126*, 11754.

(56) Moore, F. G.; Richmond, G. L. *Acc. Chem. Res.* **2008**, *41*, 739.
(57) Grimm, R. L.; Barrentine, N. M.; Knox, C. J. H.; Hemminger, J. C. *J. Phys Chem. C* **2008**, *112*, 890.
(58) Yang, J.; Meng, S.; Xu, L.; Wang, E. G. *Phys. Rev. B* **2005**, *71*, 035413.
(59) Yang, J. J.; Meng, S.; Xu, L. F.; Wang, E. G. *Phys. Rev. Lett.* **2004**, *92*, 146102.
(60) Yang, J. J.; Wang, E. G. *Phys. Rev. B* **2006**, *73*, 035406.
(61) Dubowski, Y.; Vieceli, J.; Tobias, D. J.; Gomez, A.; Lin, A.; Nizkorodov, S. A.; McIntire, T. M.; Finlayson-Pitts, B. J. *J. Phys. Chem. A* **2004**, *108*, 10473.
(62) McIntire, T. M.; Lea, A. S.; Gaspar, D. J.; Jaitly, N.; Dubowski, Y.; Li, Q. Q.; Finlayson-Pitts, B. J. *Phys. Chem. Chem. Phys.* **2005**, *7*, 3605.
(63) McIntire, T. M.; Smalley, S. R.; Newberg, J. T.; Lea, A. S.; Hemminger, J. C.; Finlayson-Pitts, B. J. *Langmuir* **2006**, *22*, 5617.
(64) Fiegland, L. R.; Saint Fleur, M. M.; Morris, J. R. *Langmuir* **2005**, *21*, 2660.
(65) Thomas, E. R.; Frost, G. J.; Rudich, Y. *J. Geophys. Res., [Atmos.]* **2001**, *106*, 3045.
(66) Voges, A. B.; Stokes, G. Y.; Gibbs-Davis, J. M.; Lettan, R. B.; Bertin, P. A.; Pike, R. C.; Nguyen, S. T.; Scheidt, K. A.; Geiger, F. M. *J. Phys. Chem. C* **2007**, *111*, 1567.
(67) Sagiv, J. *J. Am. Chem. Soc.* **1980**, *102*, 92.
(68) Lemieux, R. U.; von Rudloff, E. *Can. J. Chem.* **1955**, *33*, 1701.
(69) Lemieux, R. U.; von Rudloff, E. *Can. J. Chem.* **1955**, *33*, 1710.
(70) Wasserman, S. R.; Tao, Y. T.; Whitesides, G. M. *Langmuir* **1989**, *5*, 1074.
(71) Mar, W.; Klein, M. L. *Langmuir* **1994**, *10*, 188.
(72) Yamamoto, H.; Watanabe, T.; Ohdomari, I. *J. Chem. Phys.* **2008**, *128*, 164710.
(73) Ulman, A. *Chem. Rev.* **1996**, *96*, 1533.
(74) Allara, D. L.; Parikh, A. N.; Rondelez, F. *Langmuir* **1995**, *11*, 2357.
(75) Porter, M. D.; Bright, T. B.; Allara, D. L.; Chidsey, C. E. D. *J. Am. Chem. Soc.* **1987**, *109*, 3559.
(76) Fenter, P.; Eisenberger, P.; Liang, K. S. *Phys. Rev. Lett.* **1993**, *70*, 2447.
(77) Tidswell, I. M.; Rabedeau, T. A.; Pershan, P. S.; Kosowsky, S. D.; Folkers, J. P.; Whitesides, G. M. *J. Chem. Phys.* **1991**, *95*, 2854.
(78) Parikh, A. N.; Allara, D. L.; Azouz, I. B.; Rondelez, F. *J. Phys. Chem.* **1994**, *98*, 7577.
(79) Whitesides, G. M.; Laibinis, P. E. *Langmuir* **1990**, *6*, 87.
(80) Feller, S. E.; MacKerell, A. D. *J. Phys. Chem. B* **2000**, *104*, 7510.
(81) Szőri, M.; Tobias, D. J.; Roeselová, M. *J. Phys Chem. B*, submitted for publication.
(82) Vieceli, J.; Ma, O. L.; Tobias, D. J. *J. Phys. Chem. A* **2004**, *108*, 5806.
(83) Berendsen, H. J. C.; Grigera, J. R.; Straatsma, T. P. *J. Phys. Chem.* **1987**, *91*, 6269.
(84) Phillips, J. C.; Braun, R.; Wang, W.; Gumbart, J.; Tajkhorshid, E.; Villa, E.; Chipot, C.; Skeel, R. D.; Kale, L.; Schulten, K. *J. Comput. Chem.* **2005**, *26*, 1781.
(85) Essmann, U.; Perera, L.; Berkowitz, M. L.; Darden, T.; Lee, H.; Pedersen, L. G. *J. Chem. Phys.* **1995**, *103*, 8577.
(86) Ryckaert, J. P.; Ciccotti, G.; Berendsen, H. J. C. *J. Comput. Phys.* **1977**, *23*, 327.
(87) Brown, E. C.; Mucha, M.; Jungwirth, P.; Tobias, D. J. *J. Phys. Chem. B* **2005**, *109*, 7934.
(88) Humphrey, W.; Dalke, A.; Schulten, K. *J. Mol. Graphics* **1996**, *14*, 33.
(89) Angst, D. L.; Simmons, G. W. *Langmuir* **1991**, *7*, 2236.
(90) Engquist, I.; Lundstrom, I.; Liedberg, B. *J. Phys. Chem.* **1995**, *99*, 12257.
(91) Zhang, Q.; Zhang, Q.; Archer, L. A. *J. Phys. Chem. B* **2006**, *110*, 4924.
(92) Weis, D. D.; Ewing, G. E. *Anal. Chem.* **1998**, *70*, 3175.
(93) Hautman, J.; Klein, M. L. *Phys. Rev. Lett.* **1991**, *67*, 1763.
(94) Vieceli, J.; Benjamin, I. *J. Phys. Chem. B* **2002**, *106*, 7898.
(95) Du, Q.; Freysz, E.; Shen, Y. R. *Science* **1994**, *264*, 826.
(96) Aarts, I. M. P.; Pipino, A. C. R.; Hoefnagels, J. P. M.; Kessels, W. M. M.; van de Sanden, M. C. M. *Phys. Rev. Lett.* **2005**, 95.
(97) Su, X.; Lianos, L.; Shen, Y. R.; Somorjai, G. A. *Phys. Rev. Lett.* **1998**, *80*, 1533.
(98) Diez-Perez, I.; Luna, M.; Teheran, F.; Ogletree, D. F.; Sanz, F.; Salmeron, M. *Langmuir* **2004**, *20*, 1284.
(99) Ong, T. H.; Davies, P. B.; Bain, C. D. *Langmuir* **1993**, *9*, 1836.
(100) Brudermann, J.; Melzer, M.; Buck, U.; Kazimirski, J. K.; Sadlej, J.; Buch, V. *J. Chem. Phys.* **1999**, *110*, 10649.
(101) Ohno, K.; Okimura, M.; Akai, N.; Katsumoto, Y. *Phys. Chem. Chem. Phys.* **2005**, *7*, 3005.
(102) Auer, B.; Kumar, R.; Schmidt, J. R.; Skinner, J. L. *Proc. Natl. Acad. Sci. U.S.A.* **2007**, *104*, 14215.
(103) Schmidt, D. A.; Milki, K. *J. Phys. Chem. A* **2007**, *111*, 10119.
(104) Chattoraj, D. K.; Birdi, K. S. *Adsorption and the Gibbs Surface Excess*; Plenum Press: New York, 1984.
(105) Winter, N.; Vieceli, J.; Benjamin, I. *J. Phys. Chem. B* **2008**, *112*, 227.
(106) Downing, H. D.; Williams, D. *J. Geophys. Res.* **1975**, *80*, 1656.
(107) Toon, O. B.; Tolbert, M. A.; Koehler, B. G.; Middlebrook, A. M.; Jordan, J. *J. Geophys. Res.* **1994**, *99*, 25631.
(108) Becraft, K. A.; Richmond, G. L. *J. Phys. Chem. B* **2005**, *109*, 5108.
(109) Hopkins, A. J.; McFearin, C. L.; Richmond, G. L. *Curr. Opin. Solid State Mater. Sci.* **2005**, *9*, 19.
(110) Hore, D. K.; Walker, D. S.; MacKinnon, L.; Richmond, G. L. *J. Phys. Chem. C* **2007**, *111*, 8832.
(111) Hore, D. K.; Walker, D. S.; Richmond, G. L. *J. Am. Chem. Soc.* **2008**, *130*, 1800.
(112) McFearin, C. L.; Richmond, G. L. *J. Mol. Liq.* **2007**, *136*, 221.
(113) Buch, V. *J. Phys. Chem. B* **2005**, *109*, 17771.
(114) Lee, C. Y.; McCammon, J. A.; Rossky, P. J. *J. Chem. Phys.* **1984**, *80*, 4448.
(115) Katrib, Y.; Martin, S. T.; Hung, H. M.; Rudich, Y.; Zhang, H. Z.; Slowik, J. G.; Davidovits, P.; Jayne, J. T.; Worsnop, D. R. *J. Phys. Chem. A* **2004**, *108*, 6686.
(116) Moise, T.; Rudich, Y. *J. Geophys. Res., [Atmos.]* **2000**, *105*, 14667.
(117) Hallen, M. A.; Hallen, H. D. *J. Phys. Chem. C* **2008**, *112*, 2086.
(118) Socrates, G. *Infrared and Raman Characteristic Group Frequencies*, 3rd ed.; John Wiley & Sons Ltd: New York, 2001.
(119) Dubois, L. H.; Zegarski, B. R.; Nuzzo, R. G. *J. Am. Chem. Soc.* **1990**, *112*, 570.
(120) Engquist, I.; Lundstrom, I.; Liedberg, B.; Parikh, A. N.; Allara, D. L. *J. Chem. Phys.* **1997**, *106*, 3038.
(121) Nuzzo, R. G.; Zegarski, B. P.; Korenic, E. M.; Dubois, L. H. *J. Phys. Chem.* **1992**, *96*, 1355.
(122) Bertilsson, L.; Potje-Kamloth, K.; Liess, H. D. *Thin Solid Films* **1996**, *285*, 882.
(123) Dubois, L. H.; Zegarski, B. R.; Nuzzo, R. G. *Proc. Natl. Acad. Sci. U.S.A.* **1987**, *84*, 4739.
(124) Duffy, D. M.; Harding, J. H. *Langmuir* **2005**, *21*, 3850.
(125) Engquist, I.; Lestelius, M.; Liedberg, B. *Langmuir* **1997**, *13*, 4003.
(126) Engquist, I.; Lestelius, M.; Liedberg, B. *J. Phys. Chem.* **1995**, *99*, 14198.
(127) Dejong, A. M.; Niemantsverdriet, J. W. *Surf. Sci.* **1990**, *233*, 355.
(128) Redhead, P. A. *Vacuum* **1962**, *12*, 203.
(129) Nuzzo, R. G.; Dubois, L. H.; Allara, D. L. *J. Am. Chem. Soc.* **1990**, *112*, 558.
(130) Karagulian, F.; Lea, A. S.; Dilbeck, C. W.; Finlayson-Pitts, B. J. *Phys. Chem. Chem. Phys.* **2008**, *10*, 528.
(131) Dick, W. D.; Saxena, P.; McMurry, P. H. *J. Geophys. Res.* **2000**, *105*, 1471.
(132) Ellison, G. B.; Tuck, A. F.; Vaida, V. *J. Geophys. Res., [Atmos.]* **1999**, *104*, 11633.
(133) Voss, L. F.; Bazerbashi, M. F.; Beekman, C. P.; Hadad, C. M.; Allen, H. C. *J. Geophys. Res., [Atmos.]* **2007**, *112*, D06209.

JP808710N